# Three-Dimensional Myoarchitecture of the Bovine Tongue Demonstrated by Diffusion Spectrum Magnetic Resonance Imaging With Tractography

**RICHARD J. GILBERT,[1]* VAN J. WEDEEN,[2] LEE H. MAGNUSSON,[1] THOMAS BENNER,[2] RUOPENG WANG,[2] GEORGE DAI,[2] VITALY J. NAPADOW,[2] AND KENNETH K. ROCHE[1]**

[1]Department of Mechanical Engineering, Massachusetts Institute of Technology, Cambridge, Massachusetts

[2]Athinoula A. Martinos Center for Biomedical Imaging, Massachusetts General Hospital, Boston, Massachusetts

ABSTRACT

The anatomy of the mammalian tongue consists of an intricate array of variably aligned and extensively interwoven muscle fibers. As a result, it is particularly difficult to resolve the relationship between the tongue's microscopic anatomy and tissue-scale mechanical function. In order to address this question, we employed a method, diffusion spectrum imaging (DSI) with tractography, for displaying the macroscopic orientational properties of the tissue's constituting myofibers. DSI measures spatially variant proton displacement for a given 3D imaging segment (voxel), reflecting the principal orientation(s) of its myofibers. Tractography uses the angular similarity displayed by the principal fiber populations of multiple adjacent voxels to generate tract-like structures. DSI with tractography thus defines a unique set of tracts based on the net orientational behavior of the myofiber populations at different positions in the tissue. By this approach, we demonstrate a novel myoarchitectural pattern for the bovine tongue, consisting of short and orthogonally aligned crossing fiber tracts in the intrinsic core region, and longer, parallel-aligned fiber tracts on the tissue margins and in the regions of extrinsic fiber insertion. The identification of locally aligned myofiber populations by DSI with tractography allows us to reconsider lingual anatomy, not in conventional microscopic terms, but as a set of heterogeneously aligned and macroscopically resolved myofiber tracts. We postulate that the properties associated with these myofiber tracts predict the mechanical behavior of the tissue and thus constitute a method to relate structure and function for anatomically complex muscular tissues. Anat Rec Part A, 288A:1173–1182, 2006. 

**Key words: lingual structural imaging; continuum model; lingual deformation; magnetic resonance imaging**

Determining the relationship between microscopic anatomy and macroscopic deformation in muscular organs remains one of the signature problems in biomechanics. While it is straightforward to relate structure to function where myofibers are aligned parallel to each other, it is difficult to predict how tissues should deform when their constituting fibers exhibit microscopic crossing or convergence. Such anatomical complexity is, in fact, common in tissues such as the tongue (Sonntag, 1925; Abd-El-Malkek, 1939; Miyawaki, 1974: Barnwell,

The first two authors contributed equally to the research represented in this study.

*Correspondence to: Richard J. Gilbert, Department of Mechanical Engineering, Massachusetts Institute of Technology, 77 Massachusetts Avenue, Cambridge, MA 02139. Fax: 781-622-5090. E-mail: rgilbert@mit.edu

Received 27 February 2006; Accepted 26 June 2006

DOI 10.1002/ar.a.20387

Published online 9 October 2006 in Wiley InterScience (www.interscience.wiley.com).

1976; Gilbert et al., 1998: Nishikawa et al., 1999; Wedeen et al., 2001), blood vessels (Ostadal et al., 1975), and the heart (Reese et al., 1995; Sanchez-Quintana et al., 1995; Hsu et al., 1998). In each instance, myoarchitectural complexity at the microscopic scale confounds simple predictions of mechanical behavior at the macroscopic scale. The tongue is a particularly intriguing model for study of structure-function relationships since its myoarchitecture contains continuous arrays of crossing fibers, reflecting the structural integration of the extrinsic (possessing external attachment to bony surfaces) and intrinsic (possessing no external attachments) muscle fibers.

The mammalian tongue is a large muscular organ that fills the majority of the oral cavity (Sonntag, 1925). Its phylogenetic origins date back to prehistoric fish, where the tongue first appears as a rudimentary organ (Livingston, 1956), and is a constant feature in vertebrates above this level. In classical terms, the musculature of the tongue is divided into intrinsic muscles, including the superior and inferior longitudinalis, the transversus, and the verticalis muscles, which are wholly contained within the body of the tongue, and the extrinsic muscles, including the genioglossus, the hyoglossus, the styloglossus, and the palatoglossus muscles, which possess bony attachments outside the tongue proper. The tongue rests on a muscular floor composed of the geniohyoid muscle, which runs in the mid-sagittal plane from the mental spine of the mandible to the body of the hyoid bone, and the mylohyoid, which runs from the mylohyoid line of the mandible to the raphe and body of the hyoid bone. While these muscle delineations are readily apparent at the point of extrinsic attachment to bony surfaces, the distinction between the intrinsic and extrinsic musculature breaks down at the point of insertion into the tongue body (Depaul and Abbs, 1996; Mu and Sanders, 1999; Napadow et al., 2001; Takemoto, 2001; Wedeen et al., 2001). In fact, the tongue's myofibers become so extensively interwoven within its body that it may be appropriate to consider the tongue not as a set of anatomically discrete fibers, but as a continuous array of fibers with varying orientations and mechanical properties.

Defining structure-function relationships for the tongue requires knowledge of 3D lingual fiber orientation at both the microscopic and macroscopic scale, and a method capable of translating such anatomical data into the biomechanical realm. Determining 3D myoarchitecture by light microscopy requires meticulous dissection and multislice reconstruction (McLean and Prothero, 1992). The major limitations of this approach stem from the inability of conventional histology to resolve through-plane fiber angle accurately, as well as the difficulty in assembling local orientational data obtained over large spatial scales into a coherent tissue-scale atlas. To address this question, we have examined lingual fiber organization by determining spatially variant water molecule self-diffusivity with diffusion-weighted nuclear magnetic resonance (NMR) imaging (Gilbert et al., 1998; Napadow et al., 2001; Wedeen et al., 2001), a technique that measures molecular diffusion as a function of direction-specific MR signal attenuation. Owing to the fact that maximal diffusion occurs parallel to the axis of most fiber-type cells, diffusion measurements can, in general, be used to derive information regarding 3D fiber orientation in whole tissue.

In the current study, we have employed a variation on the above diffusion-weighted methods, termed diffusion spectrum imaging (DSI), to resolve intravoxel complexity of fiber orientation characteristic for the tongue (Wedeen et al., 2000; Tuch, 2002; Lin et al., 2003; Gilbert et al., 2006). We combined this method with tractography (Basser, 1998), a method defining macroscopic scale geometric associations of fibers on the basis of the similarity of their alignment from one location to another in the tissue. The use of DSI with tractography thus allows us to redefine lingual anatomy in terms of novel macroscopic tract-like structures, which we postulate will provide the structural underpinnings of mechanical function within the body of the tongue.

## MATERIALS AND METHODS

### Diffusion-Weighted Imaging of Tissue Myoarchitecture

MRI has the capacity to image three-dimensional structures in whole tissue nondestructively, a capability obtained by the application of diffusion-weighted imaging methods (Torrey, 1956; Stejskal, 1965; Stejskal and Tanner, 1965; Cory and Galloway, 1990; Moseley et al., 1990; Callaghan, 1993). Diffusion is a physical property, which represents the random translational motion of water molecules in tissue, and is principally affected by the location of diffusional barriers. In muscular tissue, diffusion is greatest along the direction of individual or populations of fibers due to their elongated and cylindrically symmetric geometry. Signal attenuation receives contributions from both intracellular and extracellular fluid; however, the explicit shape of muscle cells ensures that both components induce maximal attenuation along the long axis of the myofiber. As a result of these considerations, diffusion measurements can be used to derive information regarding three-dimensional fiber orientation in situ (Fig. 1). Stejskal and Tanner (1965) solved

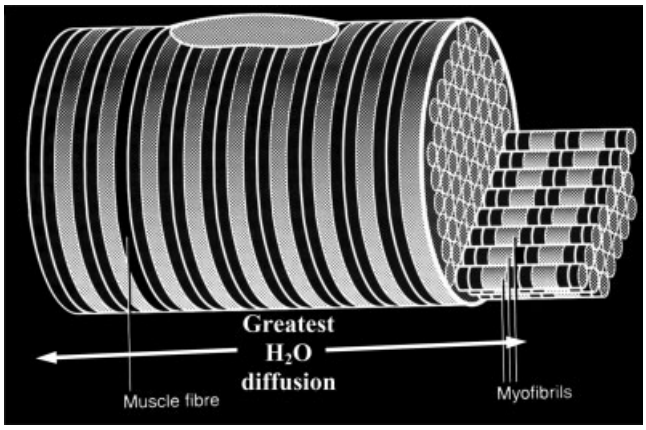


Fig. 1. Molecular diffusion in the setting of skeletal muscular tissue. Shown is a model set of aligned skeletal muscle fibers, representing the preferred direction of molecular diffusion. Due to the fact that muscle fibers are characteristically elongated and cylindrically shaped and possess a semipermeable sarcolemma, water will diffuse more readily along the fiber axis than perpendicular to the fiber axis. The inherent anisotropy of diffusion at the level of the individual fiber, or parallel bundle of fibers, provides the basis for inferring myoarchitecture on the basis of directional differences of diffusivity.

for the amount of diffusion attenuation due to an applied diffusion weighting gradient $\vec{g}$ of duration δ:

$$M(\vec{q},\Delta) = M(\vec{0},\Delta)\int \overline{P}(\vec{R}|\Delta)\exp(i\vec{q}\cdot\vec{R})d\bar{R}$$
$$\vec{q} = \gamma\vec{g}\delta \quad (1)$$

where $\vec{q}$ is called the q-value, γ is the proton gyromagnetic ratio for a water molecule, M is the signal intensity, Δ is the diffusion time, $\vec{R}$ is the diffusion distance, and $\overline{P}$ is the average probability distribution function of diffusion (PDF). It is also worthwhile to note an additional term, the b-value, which relates to the maximum overall diffusion weighting for a set of diffusion-weighted image acquisitions (Basser et al., 1994):

$$b = \|\vec{q}_{\max}\|^2\Delta \quad (2)$$

By combining the signal attenuation obtained from the application of diffusion weighting gradients in multiple directions with standard MRI image acquisition, the amount of diffusion in those directions may be measured for each voxel in the MR image. The voxels may then be reconstructed to constitute 3D representations of the tissue's underlying myoarchitecture.

## Diffusion Spectrum Imaging

DSI is a method for determining the average amount of molecular diffusion occurring within any enclosed space, such as the set of myofibers. The goal of DSI is to reconstruct the PDF for diffusion in each voxel. DSI accomplishes this by acquiring a full sampling of diffusion weighting gradient directions and magnitudes, which permits direct reconstruction of the average PDF (Fig. 2) (Wedeen et al., 2000). In this article, we use the term PDF to refer to the observed average distribution obtained from DSI processing of the signal. The use of DSI for imaging lingual fiber populations has been previously described (Gilbert et al., 2006). In brief, during DSI, diffusion-weighted images are acquired for a sphere of q vectors with indexed values in a Cartesian grid in q-space in order to produce a three-dimensional probability distribution. The PDF, $\overline{P}(\vec{R},\Delta)$, is the inverse Fourier transform of Equation 1:

$$\overline{P}(\vec{R},\Delta) = F^{-1}[M(\vec{q},\Delta)] \quad (3)$$

where $F^{-1}$ denotes the inverse Fourier transform. The spacing between $\vec{q}$ vectors defines the field of view and the maximum $\vec{q}$ vector defines the resolution of the PDF. The values of $M(\vec{q},\Delta)$ are placed in a matrix with indexes given by the indexes of the $\vec{q}$ vectors, and then the 3D inverse discrete Fourier transform is computed, producing the PDF. By measuring the microscopically resolved 3D diffusion function, DSI is able to show complex fiber relationships in terms of the multimodal behavior of the PDF within a macroscopically resolved segment of tissue.

Since the 3D PDF represents a spatial volume, it is necessary to reduce its dimensions to allow visualization and to determine the local maxima of diffusion. The method typically employed in DSI is to integrate radially the PDF by the magnitude of $\vec{R}$:

$$\mathrm{ODF}(\hat{u},\Delta) = \int \vec{P}(\rho\hat{u},\Delta)\rho\hat{u}d\rho \quad (4)$$

where $\hat{u}$ is a unit vector in the direction of $\vec{R}$. This produces a probability distribution that is a function of fiber angle and is weighted to better show long diffusion distances. This new data set is termed the orientational distribution function (ODF) and provides a probability distribution for diffusion for a set of directions, regardless of the magnitude of the diffusion. To simplify visualization further, the ODF is normalized by subtracting the smallest magnitude value. The ODF is then plotted with colors corresponding to direction and magnitude, and radii are defined by the values of the ODF. The 3D vector directions of maximum diffusion (and thus muscle fiber directions) in the voxel are then given as a function of the local maxima in the ODF.

## DSI Tractography

Each voxel in a DSI data set has one or more local maxima (the local maxima of the ODF), which defines one or more 3D vectors for each voxel in the set of images. Constructing connections along the vector directions in a vector field is accomplished by determining a set of streamlines. Mathematically, a streamline is defined as the solution of the following differential equation:

$$\frac{d\vec{S}(s)}{ds} = \vec{v}(\vec{S}(s)) \quad (5)$$

where $\vec{S}(s)$ is the streamline, s is a path coordinate along $\vec{S}$, and $\vec{v}$ is the vector field. Equation 5 demonstrates that the streamline will be tangent to the vector field at all points. Generating streamlines corresponding to a vector field in biological data has been termed tractography (Basser, 1998), since the initial use of this technique was for determining white matter tracts in the brain. Since there can be more than one local maxima per voxel, we have employed a method derived from the theory of generalized streamlines (Daivis and Coelho, 2000). Generalized streamline tractography operates by adding a constraint to the streamlines that a certain angular threshold must be met to establish intervoxel connectivity. If that threshold is met, then the tract will continue into the adjacent voxel. If, however, the threshold is not met, the tract will stop. In the instance where a tract happens on a voxel with two or more vectors that meet the angular threshold criteria, then the tract will continue along the vector of least angular difference compared with itself. In the current work, we employed an angular threshold of $< \pm 17.5^\circ$ to define tract continuity. The myofiber tract is derived from the principal fiber directions, represented as the directions of maximum diffusion of the ODF, in a set of adjacent voxels. The DSI tracts are displayed using custom software developed using VTK, an open-source 3D visualization tool (http://www.vtk.org/; Fig. 3). To illustrate further the generation of myofiber tracts in actual tissue, we show in Figure 4 a characteristic set of fiber tracts from a mid-sagittal slice of the bovine tongue, in which the myofiber tracts and the underlying DSI ODFs, from which the tracts are derived, are displayed in the same image. The myofiber tracts so identified do not necessarily correspond to conventional anatomical entities, such as fiber bundles or fascicles. In the current context, the

tract is a macroscopic representation of multiple fibers or bundles within a segment of tissue that share similar orientation. To quantify tract angle, tract position is determined at two consecutive points along the tract, thus dividing the tract up into segments. The x, y, and z coordinates of each segment are subtracted and divided by the length of the segment, thus identifying the segment's 3D orientation. These segment orientations are colored based on direction and then represented on a spherical graph, with graph center being (0, 0, 0).

### Image Acquisition Protocol

Imaging was performed with a Siemens Allegra 3T scanner on eight ex vivo cow tongues obtained from Blood Farms (West Groton, MA). Whole specimens were refrigerated and scanned within 24 hr of harvest. The imaging protocol employed a diffusion gradient sampling scheme, which consisted of a keyhole Cartesian acquisition to include q-space values lying on a Cartesian grid for a total of 515 sampling points. Typical image matrix sizes were $64 \times 64 \times 25$ with voxel resolutions of 2.8–4 $mm^3$. The b-values used were in the range of 5,500–8,500 $s/mm^2$.

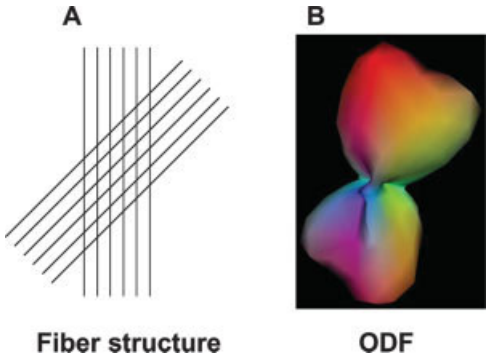


Fig. 2. Visualization of 3D fiber architecture by DSI. Displayed is the method by which DSI infers 3D fiber structure from direction-specific diffusivity for a given voxel. The PDF for diffusion is reconstructed by taking the 3D Fourier transform of the entire set diffusion values and then converted to the ODF, providing a probability distribution for diffusion for set angular directions independent of magnitude. **A:** The relationship between two model fiber populations (all fibers within a population being parallel) at a given angular relationship to each other. **B:** ODF corresponding to the set of crossing fibers. Note that the diffusion maxima of the PDF correspond to the directions of greatest diffusion, which is a determinant of fiber orientation.

## RESULTS

The images shown in this article are representative of those obtained from a set of adult bovine tongues ($n = 8$ tongues). For ease of visualization, the DSI tractography images display only those tracts passing through a designated plane. Thus, we show only a subset of all the tracts in a given data set in each image. The color-coding is the same in all images, regardless of the slice orientation, and is depicted as follows: green indicates tracts in the anterior-posterior direction (longitudinal orientation of the tissue), blue indicates the side-to-side direction (transverse orientation of the tissue), and red indicates the superior-inferior direction (vertical direction of the tissue).

Figure 5 depicts the myofiber populations passing through a mid-sagittal plane from opposite lateral perspectives. Since the tracts represent only the tracts passing through a mid-sagittal plane, the lateral portions of the tongue, and the associated fiber tracts, are largely cut away. Owing to the fact that the tracts were obtained directly from DSI data, they are a statistical representation of the set of similarly aligned fibers across multiple voxels. While these tracts tend to correlate well with several classically defined extrinsic and intrinsic muscles, the tracts also display novel attributes of the tissue geometry. The individual tract depicts a unique population of myofibers, independent of their point of origin (i.e., extrinsic vs. intrinsic), which is defined at the macroscopic (or tissue) scale by the similarity of their alignment. In general, the longitudinal

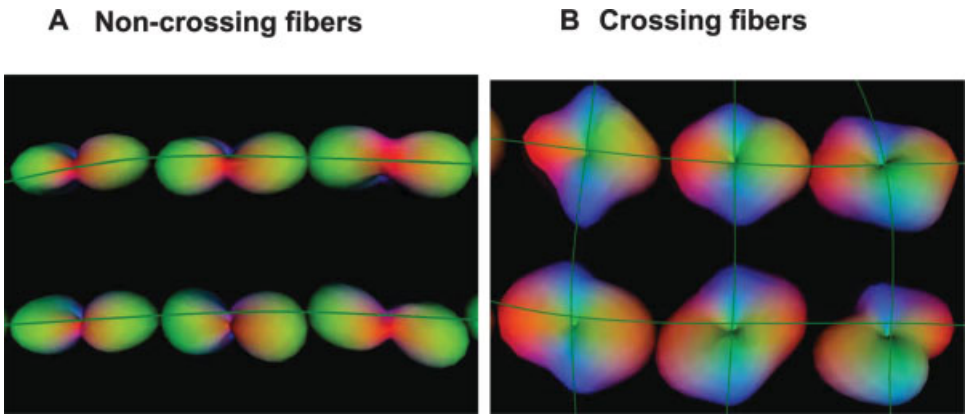


Fig. 3. Determination of intervoxel fiber relationships with DSI tractography. Depicted here is the method by which intervoxel fiber association, i.e., tract formation, is determined on an actual set of ODFs derived from various regions of the bovine tongue employing DSI. Intervoxel association was determined by the method of generalized streamline tractography. By this method, if a certain angular threshold (35° in the current project) relating the direction of maximum diffusion of one voxel to another is achieved, connectivity is inferred. On the other hand, if this angular threshold is not achieved, connectivity does not exist, and tract extension ceases. **A:** Set of actual ODFs and tracts obtained from the superior surface of the tongue, where fibers are aligned in a single direction. **B:** Set of ODFs and tracts obtained from the lingual core, where fibers are aligned in two orthogonal directions.

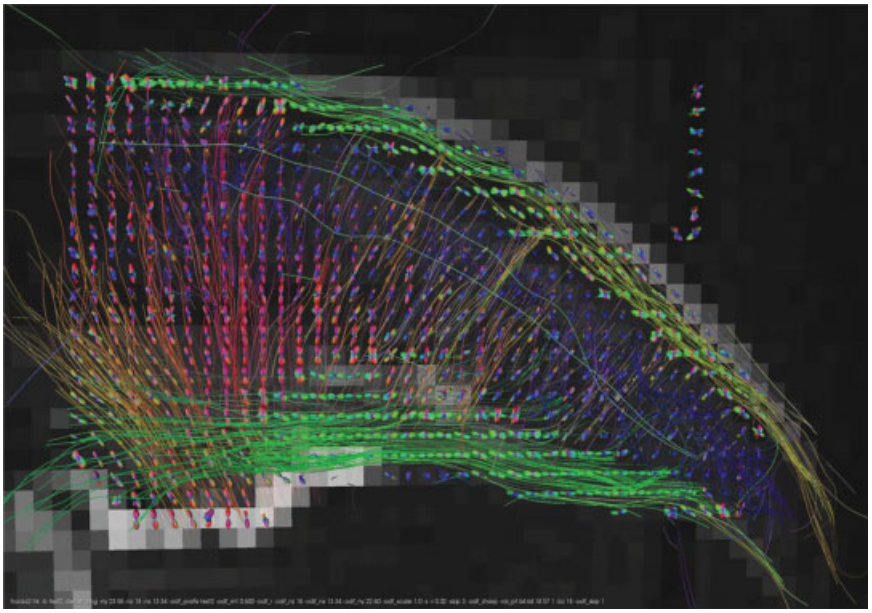

Fig. 4. Generation of DSI myofiber tracts in a mid-sagittal slice. Shown is a mid-sagittal slice from the bovine tongue in which the ODFs obtained by DSI are depicted in the same image as the myofiber tracts derived from the principal fiber directions of the ODFs. In subsequent images, the myofiber tracts are displayed in the absence of the underlying DSI ODFs. All fibers contained within this imaging plane are depicted.

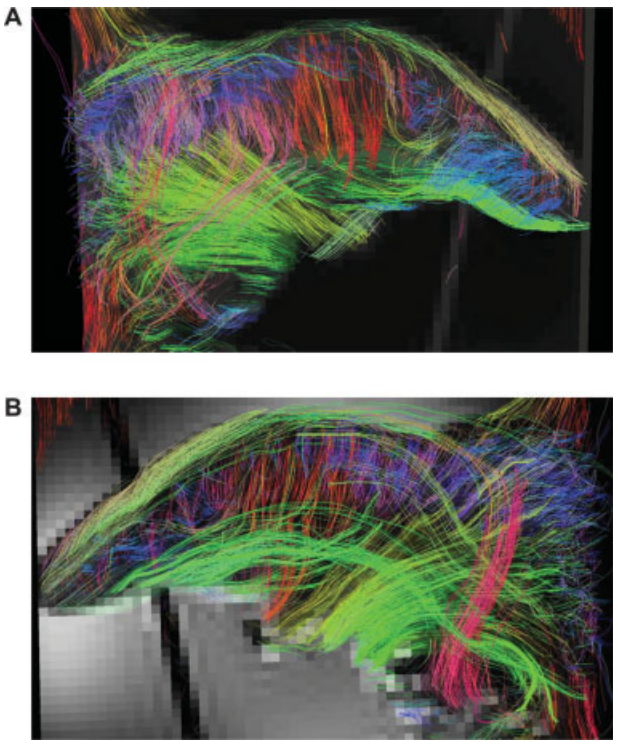


Fig. 5. DSI tractography of tongue (mid-sagittal orientation). Shown are myofiber populations depicted as tracts passing through a mid-sagittal plane of the bovine tongue viewed from opposite orientations. DSI tractography connects the maximum intravoxel coherences between adjacent voxels, which constitutes a set of similarly aligned fiber populations, or tracts. **A:** Anterior tip to the right. **B:** Anterior tip to the left. Tract orientation is displayed per the color code in the 3D reference sphere. Green fibers correspond to the longitudinally oriented fibers on the superior and inferior surfaces of the tissue, and the longitudinally aligned fibers of the genioglossus. The core region of the tissue displays horizontally aligned transversus fiber tracts, vertically aligned fiber tracts associated with the verticalis and genioglossus fiber tracts.

sheath fibers are depicted as long tracts (shown in green) sandwiching the lingual core. The lingual core is most distinct in the anterior portion of the tissue, but in fact persists into the posterior portion of the tissue as well. The lingual core is comprised of distinct transversus tracts (shown in blue) and vertically oriented tracts (shown in red). Notably, one cannot distinguish if these vertically oriented tracts correspond in fact to the verticalis or to vertically aligned genioglossus myofibers. There is a set of large midline fiber tracts, which fan out radially from a medial connection on the mandible bone into the core of the tongue, likely to correspond to the genioglossus fibers, and which merge with the vertically aligned tracts. In addition, there is separate vertically aligned set of fiber tracts, which originates at a posterior medial connection on the hyoid bone, and then courses laterally and vertically, and finally merges with lateral longitudinal fibers. These latter myofibers are likely to correlate with the hyoglossus. We demonstrate in Figure 6 an obliquely oriented image in which the superior aspect of the longitudinalis is removed, demonstrating the relationship between the laterally located longitudinally oriented sheath fibers (green), the transversely oriented transversus fibers, and the vertically oriented fibers (red and orange) comprised by the verticalis and genioglossus.

The geometry of several of these fiber tracts may be accentuated by electing to use alternative planes of reference. In Figure 7A, we show in more detail the fiber tracts traversing a horizontal reference plane in order to emphasize the varying angles exhibited by the verticalis and vertically oriented genioglossus as they project to the superior surface of the tissue. The longitudinal sheath of the tongue is still visible in green, but in this view, mainly the lateral tracts are present and the inferior and superior populations have been cut away. A small population of longitudinally oriented fiber tracts is observed to enter posteriorly and superiorly, coursing lateral to the apparent hyoglossus fiber tracts, and finally interdigitating with longitudinal fiber tracts. These fiber tracts may correlate with the styloglossus

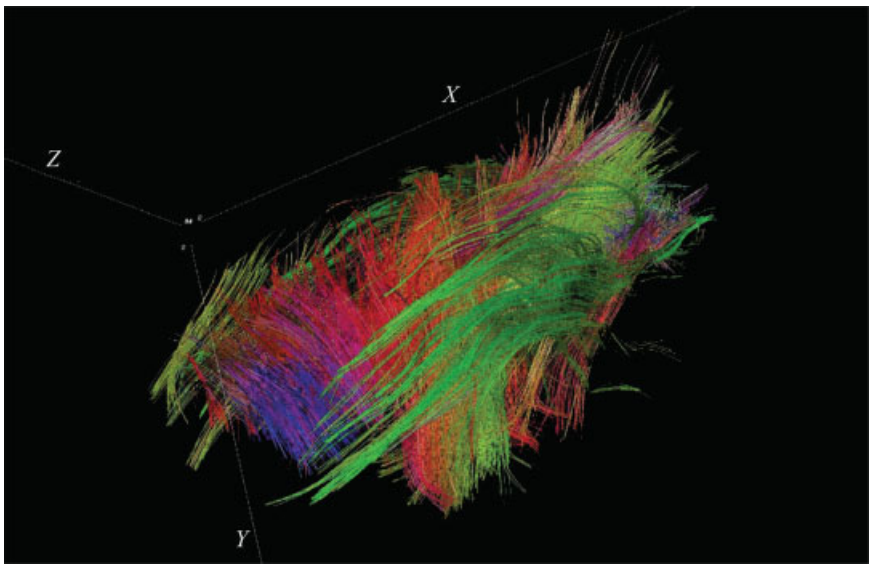


Fig. 6. DSI tractography of tongue (oblique orientation). Shown is an obliquely oriented image in which the superior aspect of the longitudinalis is removed in order to demonstrate the relationship between laterally located longitudinally oriented sheath fibers (green), with the transversely oriented transversus fibers (blue), and the vertically oriented fibers (red and orange) comprised by the verticalis and genioglossus. To display perspective in this orientation, the tongue image is depicted relative to obliquely configured x-y-z coordinates.

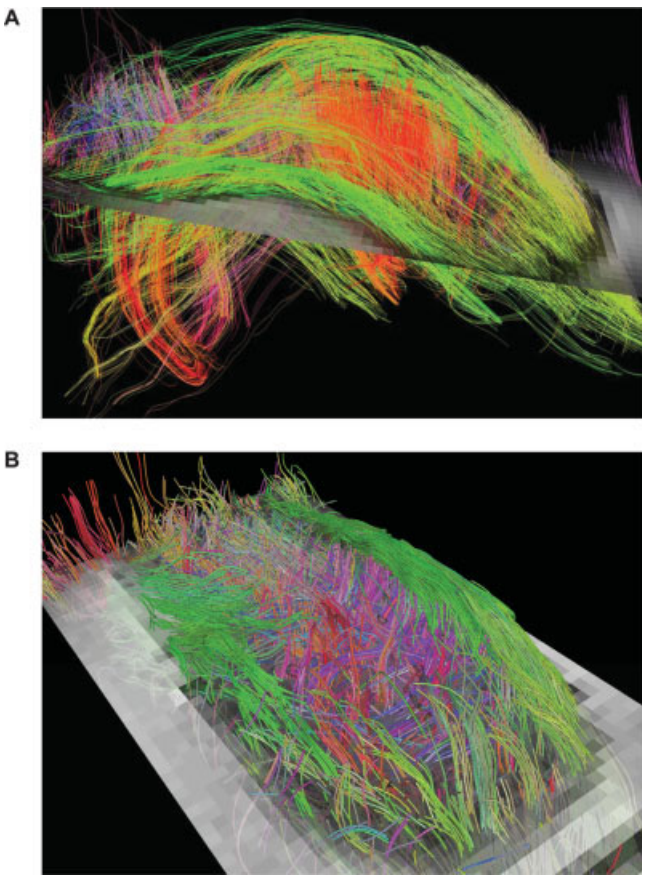


Fig. 7. DSI tractography of tongue (horizontal reference plane). Shown are DSI tractography images of the bovine tongue, in which specific fiber populations are accentuated by providing reference planes. **A:** The use of a horizontal plane of reference depicts more clearly the vertically aligned fibers of the genioglossus and verticalis (red) projecting upward to the superior surface of the tissue. **B:** Horizontal plane of reference employed in combination with the removal of the top layer of the tissue in order to display the variation in the merging and crossing of myofiber tracts in the core as a function of AP position.

fibers, although this association is more difficult to discern without the presence of the surrounding muscular anatomy. In Figure 7B, we depict the lingual fiber tracts also from the perspective of a horizontal reference plane, but orient the image so that the superior longitudinally oriented fiber tracts are cut away, displaying the crossing fiber tracts of the lingual core. We demonstrate in this image the variation in the merging and crossing of vertically oriented and transversely oriented bundles of fibers, shown in red and blue, respectively, as a function of anterior-posterior position.

The corresponding vertically aligned and transversely aligned fiber tracts in the anterior and posterior lingual core are shown in a representative set of axial slices in Figure 8. Figure 8A represents an anterior axial slice (thickness $\sim$ 2 cm). The longitudinal sheath is shown as green fibers surrounding the core and oriented out of the page. The transversus fibers are shown in blue and the verticalis as red. Interestingly, the transversely aligned fibers tend to be localized to the more superior region. In addition, the vertically aligned fibers are separated into two lateral populations with slightly oblique orientations toward the superior midline. Figure 8B represents a representative posterior slice, and demonstrates a set of posteriorly oriented (green) fiber tracts in the midline, likely to be the posterior genioglossus tracts, as well the longitudinally oriented sheath tracts, and superiorly located vertically and transversely aligned fibers. Distinct vertically aligned fiber tracts, likely to be the hyoglossus, are shown laterally in the most posterior axial image. We demonstrate (Fig. 8C) the fiber tract angles from Figure 8A quantitatively on a 3D scatter plot. This method allows us to depict the variation of tract angles on an x-y-z coordinate system, with y corresponding to the longitudinal direction, z to the vertical direction, and x to the transverse direction. The green-red-blue color scheme, employed in the above images, was continued in this graph. As predicted, there is a distinct population of tracts aligned in the longitudinal direction clustered around origin of the graph (0, $\pm$1, 0), and populations orthogonal to each other aligned in the vertical and transverse directions. The minimal

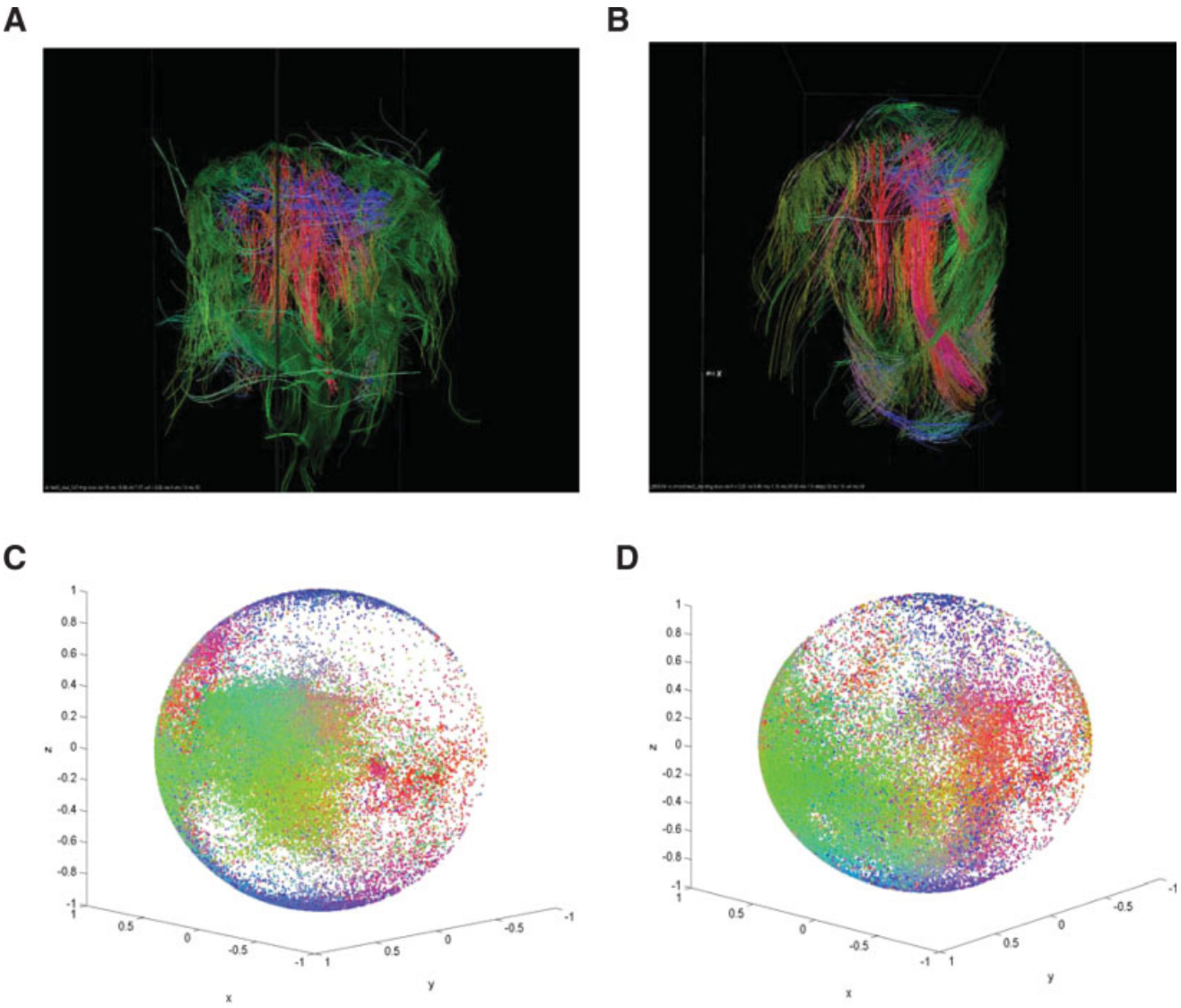


Fig. 8. DSI tractography of tongue (axial orientation). Depicted are axial slices (~2 cm thick) obtained from the anterior (**A**) and posterior tongue (**B**), and quantification of 3D myofiber tract angle for the anterior (**C**) and posterior tongue (**D**). A: Anterior tongue demonstrates longitudinally oriented fiber tracts surrounding the core region (projecting out of the page), and a lingual core consisting of transversely oriented fiber tracts (transversus) and vertically oriented fiber tracts (verticalis). Note the superior localization of the transverse fiber tracts and the separation of the vertically aligned fiber tracts into two lateral tract populations, or bundles. B: Posterior tongue showing prominent longitudinally oriented midline and sheath fiber tracts (green, directed out of page), vertically oriented (red) fiber tracts in the midline and posterolateral, and transverse oriented fiber tracts in the superior portion of the tissue. C: Anterior tongue tract angles were determined for the entire DSI tractography data set in anterior tongue segment displayed in A and displayed in a 3D scatter plot with the graph center as (0, 0, 0). The myofiber tract populations segregated into longitudinally aligned (green) tracts clustered around (0, ±1, 0), and vertical (red) and transverse (blue) tracts aligned orthogonally to each other with minimal fiber overlap. D: Posterior tongue tract angles were determined for the DSI tractography data set in the posterior tongue segment displayed in B. These data may be distinguished from that shown in C by the higher degree of angular overlap (i.e., less angular separation), consistent with the nonorthogonal relationship among the constituent fiber tracts in the posterior tongue.

degree of overlap between these populations of fiber tracts indicates that these tracts are aligned in the segment of the tissue in an explicitly orthogonal configuration. The fiber tract angles derived from Figure 8B are shown quantitatively in Figure 8D. It should be noted that there is considerably more overlap of tract angle in this case (posterior tongue) as compared to Figure 8C (anterior tongue). This is consistent with the fact that fiber tracts align more closely in an orthogonal manner in the anterior tongue, thus resulting in more apparent angular separation, as compared to the more complex angular relationships present in the posterior tongue.

## DISCUSSION

The study of lingual anatomy poses a classical dilemma: How is it possible to relate the tissue's highly complex myoarchitecture with the multitude of possible

deformations occurring during physiological motion? The extent to which lingual deformation corresponds to its underlying myoarchitecture has offered both the opportunity and the challenge to explore fundamental concepts of structure and function. We present here a novel approach, DSI with tractography, for visualizing the complex myoarchitecture of the mammalian tongue, which depicts muscular organization, not as individual myofibers but as macroscopically resolved myofiber tracts, representing similarly aligned myofiber populations. The length and orientation of an individual myofiber tract are in turn dictated by the extent (in voxels) over which myofiber orientational similarity exists in the tissue. We propose that these macroscopically defined myofiber tracts constitute a structural template, which dictates the direction of local tissue shortening during deformation. Whole tissue deformation, resulting from the net effect of such local shortening events, thus comprises the physiological basis for purposeful motion.

DSI resolves morphologically complex myoarchitecture by obtaining the average molecular diffusion function within a region of tissue and depicting it as the probability that a given water molecule will undergo direction-specific motion within a given period of time. The degree of diffusivity in a particular direction is dictated largely by the presence of physical barriers to diffusion, such as cell membranes and cytoskeletal fiber elements. The net diffusion in a tissue sample is represented as an ensemble PDF for the complete array of displacements in that region of tissue. The PDF for a given diffusion data set is specifically based on the Fourier relationship between the PDF and the diffusion signal for the spin echo obtained at various gradient strengths. Complete DSI acquisitions are assembled by fully sampling q-space, where q-space is a formalism that represents diffusion weighting as a function of the strength and direction of the magnetic field gradient applied during the MRI experiment (Wedeen et al., 2000, 2001; Tuch, 2002). This is in contrast to other diffusion weighting gradient sampling schemes, which sample only on a segment (or surface) of q-space by acquiring images based on only a limited sample of gradient strengths or directions (Basser et al., 1994; Basser, 1998; Napadow et al., 2001; Tuch, 2002). For purposes of visualization, the full 3D PDF may be converted to an ODF, which collapses the data to better display the directions of maximum diffusion. By this conversion, there are a finite number of directions in which the 3D diffusion function is sampled, which translates into the maximum possible angular resolution. Since one local point minima must separate two local maxima, the maximum possible angular resolution is within the noise threshold found in the reconstructed 3D diffusion function. Since most the crossing fibers observed in the tongue have orthogonal relationships to each other, this does not generally constitute a limitation of the ODF method. In the less common instance where fibers merge or diverge within a given voxel, i.e., possess small angular relationships, the precise angular relationship may be difficult to distinguish by observing the diffusion functions or ODFs alone, and it is the angular coherence between adjacent voxels that is important.

Tractography is a means for relating the angular coherence between voxels and relating the orientations obtained from the tissue diffusion microenvironment to the overall tissue macroenvironment. The logical underpinnings for tractography come from a desire to connect orientations, in a very similar manner to which streamlines connect vector fields in order to view trajectories in those fields. For example, a charged particle moving in a complicated magnetic field can be viewed as a streamline, thus providing a macroscale picture by knowing only the various microscale environments that particles might encounter. The goal is similar in the case of tractography, with the principal difference being that intervoxel angle similarity is also a driving factor in determining the trajectory that a tract may take. The tractography algorithm is constructed such that the tract takes the path of minimum angular difference. Consequently, the tract will stop if the angular difference between adjacent voxels is too high. Similarly, if the voxel contains two or more compatible paths, the tract will take that of the least angular difference. The exact minimum angular difference may vary with the tract construction algorithm. In the current work, we chose a minimum angular difference, which provided a reasonable depiction of the predicted macroscale myofiber relationships. This condition will, however, be systematically studied in future work in order to determine its discriminant value in determining myoarchitecture in this and other tissues.

These tracts may be considered the macroscopic representation of the population(s) of aligned myofibers within the imaged segment of tissue. Through the use of DSI with tractography, we have created a novel multiscalar metric for depicting complex myofiber populations, which represents at the same time microscopic and macroscopic myofiber orientation. In doing so, we have confirmed a number of previous notions of lingual myoarchitecture and demonstrated several novel concepts.

One, the lingual core consists of orthogonally related transversus and verticalis fibers, whose associated tracts span the distance between the superior and interior longitudinalis fibers. This property was exhibited by the distinct angular differences shown by the tract oriented longitudinally, transversely, and vertically. Differences also exist in the broad pattern of alignment exhibited by these tracts. For example, the transversus tracts are arrayed in a parallel configuration, principally in the superior portion of the tissue, whereas the verticalis tracts are configured in a way that separates into right and left tracts. The functional consequences of the latter configuration are at this point unknown.

Two, while the tracts associated with the genioglossus muscle are notable for their fan-like projection to the superior surface in the mid-sagital tongue, the vertically oriented segment of the genioglossus and the verticalis tracts per se are largely indistinguishable from each other on the basis of orientation. This suggests that in addition to the merging of microscopic anatomy, there may be a merging of mechanical function in the vertical orientation. Local fiber tract orientation may thus constitute a more appropriate determinant of local mechanical function in complex tissues than the function of one discrete muscle or another.

Three, based solely on its myoarchitecture, the tongue segregates itself into the anterior tongue, which is comprised almost completely of intrinsic fibers aligned along the principal axes, and the posterior tongue, which embodies the intrinsic fibers but incorporates fibers that originate externally, i.e., genioglossus, styloglossus, hyoglossus, and palatoglossus. It is noteworthy that the an-

terior tongue is capable of a vast array of displacements along with the institution of variable stiffening. Such properties are important both in speech and in the accommodation of a large array of bolus types. In contrast, the posterior tongue possesses a more limited repertoire of mechanical functions, yet is capable of exerting greater force to achieve certain physiological goals, such as bolus propulsion during swallowing.

The existence of overlapping and variably aligned fiber tracts supports the conceptualization of the tongue as a continuum of muscular elements. From a mechanical perspective, the tongue is believed to fall into a class of organs known as a muscular hydrostat, an organ whose musculature both creates motion and supplies the skeletal support for that motion (Kier and Smith, 1985; Smith and Kier, 1989; Napadow et al., 1999, 2002). Such organs characteristically are isovolemic, i.e., maintain their volume while undergoing various changes of shape and form, and are composed of complex fiber arrays aligned at angles orthogonal to the direction of deformation. Such fiber arrangements comprise the structural underpinnings for hydrostatic deformation and therefore are fundamental in the generation of lingual force. By definition, all hydrostats possess fibers parallel and perpendicular to the organ's long axis, but differ regarding the relative position and geometry of the perpendicular fibers. For example, muscular hydrostats that principally perform bending motions tend to have longitudinal fibers farther away from the longitudinal axis. An example of this phenomenon is the snake, which typically flicks its chemoreceptor-laden organ to sense its prey (de Groot et al., 2004). The fibers of the elephant trunk, on the other hand, are organized in a spiral fashion about the central longitudinal axis, thereby maximizing the ability of the organ to perform the twisting needed for grasping arboreal vegetation (Endo et al., 2001). The tentacle of the squid, which is most structurally similar to the mammalian tongue, has a core region of transverse fibers surrounded by a longitudinal sheath (Friel and Wainwright, 1998). The presence of structural complexity, both in terms of crossing myofibers (single voxel scale) and variably aligned myofiber tracts (multivoxel scale), as shown in this report, may be seen as an anatomical prerequisite for hydrostatic deformation.

Based on the above considerations, we postulate that these 3D aligned tracts provide a reference configuration, or mechanical template, on which deformation preferentially occurs. In this manner, it should be possible to conceive of the principal directions of contraction in a complex tissue, such as the tongue, by a superposition of tissue shortening in the directions of the indicated fiber tracts. In turn, this should allow an explicit conceptualization of macroscale mechanical function from the net microscale anatomical data set. Despite the many degrees of freedom embodied by the tongue and the large number of compatible contractions, it should be feasible to project deformed configurations from the myoarchitecture specified by DSI tractography. Several limitations of this technique should, however, be acknowledged. Since fundamentally DSI resolves fiber orientation through a determination of principal directions of diffusion, certain microscopic complexity seen at the resolution of conventional light microscopy will be missed. Whether this level of resolution is significant in terms of understanding tissue mechanics has not been determined. Furthermore, it is uncertain whether DSI tractography, at the level of angular resolution shown in this report, will be feasible in vivo due the required imaging time and the deleterious effects of gross motion on image integrity. An alternative approach, albeit with less angular precision, may be to derive intervoxel tracts based on voxel-specific principal fiber direction with high-resolution DTI.

In conclusion, we have employed a novel method, DSI tractography, for determining the orientation of variably aligned myofiber populations in the mammalian tongue. The delineation of myofiber tracts in the tongue allows us to compile a macroscale anatomic model, which can be explicitly related via the diffusion function to microscopic anatomy. We postulate that the definition of locally aligned fiber populations constitutes a measure of mechanical continuity and forms a structural template on which region-specific contractions occur under physiological conditions.

## LITERATURE CITED


Abd-El-Malkek S. 1939. Observations on the morphology of the human tongue. J Anat 73:201–210.

Barnwell YM. 1976. Human lingual musculature: a historical review. Int J Oral Myol 2:31–34.

Basser PJ, Mattiello J, et al. 1994. MR diffusion tensor spectroscopy and imaging. Biophys J 66:259–267.

Basser PJ. 1998. Fiber-tractography via diffusion tensor MRI (DT-MRI). Sydney: 6th Annual Meeting ISMRM.

Callaghan PT. 1993. Principles of nuclear magnetic resonance microscopy. Oxford: Oxford University Press.

Cory DG, Galloway AN. 1990. Measurement of translational displacement probabilities by NMR: an indicator of compartmentation. Magn Reson Med 14:435–444.

Daivis PJ, Coelho JL. 2000. Generalized Fourier law for heat flow in a fluid with a strong, nonuniform strain rate. Phys Rev E Stat Phys Plasmas Fluids Relat Interdiscip Top 61:6003–6006.

de Groot JH, van der Sluijs I, et al. 2004. A three-dimensional kinematic analysis of tongue flicking in Python molurus. J Exp Biol 207(Pt 5):827–839.

Depaul R, Abbs JH. 1996. Quantitative morphology and histochemistry of intrinsic lingual muscle fibers in *Macaca fascicularis*. Acta Anat 155:29–40.

Endo H, Hayashi Y, et al. 2001. Muscle architecture of the elongated nose in the Asian elephant (*Elephas maximus*). J Vet Med Sci 63:533–537.

Friel JP, Wainwright PC. 1998. Evolution of motor patterns in tetraodontiform fishes: does muscle duplication lead to functional diversification? Brain Behav Evol 52:159–170.

Gilbert RJ, Daftary S, et al. 1998. Determination of lingual myoarchitecture in whole tissue by NMR imaging of anisotropic water diffusion. Am J Physiol 175:G363–G369.

Gilbert RJ, Magnusson LH, et al. 2006. Mapping complex myoarchitecture in the bovine tongue with diffusion spectrum magnetic resonance imaging. Biophys J 91:1014–1022.

Hsu EW, Muzikant AL, et al. 1998. Magnetic resonance myocardial fiber-orientation mapping with direct histological correlation. Am J Physiol 274(5 Pt 2):H1627–H1634.

Kier WM, Smith KK. 1985. Tongues, tentacles and trunks: the biomechanics of movement in muscular-hydrostats. Zool J Linnean Soc 83:307–324.

Lin CP, Wedeen VJ, et al. 2003. Validation of diffusion spectrum magnetic resonance imaging with manganese-enhanced rat optic tracts and ex vivo phantoms. Neuroimage 19:482–495.

Livingston RM. 1956. Some observations on the natural history of the tongue. Ann R Coll Surg Engl 19:185–200.

McLean M, Prothero J. 1992. Determination of relative fiber orientation in heart muscle: methodological problems. Anat Rec 232: 459–465.

Miyawaki K. 1974. A study of the musculature of the human tongue. Ann Bull Res Inst Logoped Phoniatr 8:23–50.

Moseley ME, Cohen Y, et al. 1990. Early detection of regional cerebral ischemia in cats: comparison of diffusion and T2-weighted MRI and spectroscopy. Magn Reson Med 14:330–346.

Mu L, Sanders I. 1999. Neuromuscular organization of the canine tongue. Anat Rec 256:412–424.

Napadow VJ, Chen Q, et al. 1999. Intramural mechanics of the human tongue in association with physiological deformations. J Biomech 32: 1–12.

Napadow VJ, Chen Q, et al. 2001. Quantitative analysis of 3D resolved fiber architecture in heterogeneous skeletal muscle using NMR and optical imaging methods. Biophys J 80:2968–2975.

Napadow VJ, Kamm RD, et al. 2002. A biomechanical model of sagittal tongue bending. J Biomech Engineer 124:547–556.

Nishikawa KC, Kier WM, et al. 1999. Morphology and mechanics of tongue movement in the African pig-nosed Hemisus Marmoratum: a muscular hydrostatic model. J Exp Biol 202:771–780.

Ostadal B, Schiebler TH, et al. 1975. Relations between development of the capillary wall and myoarchitecture of the rat heart. Adv Exp Med Biol 53:375–388.

Reese TG, Weisskoff RM, et al. 1995. Imaging myocardial fiber architecture in vivo with magnetic resonance. Magn Reson Med 34: 786–391.

Sanchez-Quintana D, Garcia-Martinez V, et al. 1995. Morphological changes in the normal pattern of ventricular myoarchitecture in the developing human heart. Anat Rec 243:483–495.

Smith KK, Kier WM. 1989. Trunks, tongues, and tentacles: moving with skeletons of muscle. Am Sci 77:29–35.

Sonntag CF. 1925. The comparative anatomy of the tongues of mammalia: XII, summary, classification, and physiology. J Zool 21: 701–762.

Stejskal EO. 1965. Use of spin echoes in a pulsed magnetic-field gradient to study anisotropic, restricted diffusion and flow. J Chem Phys 48:3597–3603.

Stejskal EO, Tanner JE. 1965. Spin diffusion measurements: spin echoes in the presence of a time-dependent field gradient. J Chem Phys 42:288–292.

Takemoto H. 2001. Morphological analyses of the human tongue musculature for three-dimensional modeling. J Speech Lang Hear Res 104:563–565.

Torrey HC. 1956. Bloch equations with diffusion terms. Phys Rev 104: 563–565.

Tuch DS. 2002. Diffusion MRI of complex tissue structure. PhD thesis. Cambridge, MA: Massachusetts Institute of Technology.

Wedeen VJ, Reese TG, et al. 2000. Mapping fiber orientation spectra in cerebral white matter with Fourier-transform diffusion MRI. Denver, CO: 8th Annual Meeting ISMRM.

Wedeen VJ, Reese TG, et al. 2001. Demonstration of primary and secondary fiber architecture of the bovine tongue by diffusion tensor magnetic resonance imaging. Biophys J 80:1024–1028.